Electromagnet Design for Microscale Vessels

Nail Akçura
Mechatronics Engineering Dept.
Dokuz Eylül University
İzmir, Turkey
nailakcura@gmail.com

Levent Çetin
Mechatronics Engineering Dept.
İzmir Katip Çelebi University
İzmir, Turkey
levent.cetin@ikc.edu.tr

Özgür Tamer
Electrical and Electronics Dept.
Dokuz Eylül University
İzmir, Turkey
ozgur.tamer@deu.edu.tr

***Abstract*— Helmholtz coils are used for generating uniform magnetic field comprising a workspace between two identically symmetric coils. These Helmholtz coil based structure can be used for excitation of micro scaled robots [1]. With the aid of this external effect, force and torque can be generated over the micro robot. Owing to the dimensions of the robot, it can be used through veins in medical operations [2][3]. With the developing technology, it is predicted to use micro/nano scale producible robots with several functions in medical operations. Taking this system to a feasible state can be assumed as a revolutionary progress. In this paper, an electromagnet design is examined depending on the results of the magnetic field. Homogeneity of the 2-D working space takes the priority in the study. Depending on the analyzes, cost-gain ratios between the dimension of the homogeneity at different current levels, the magnetic flux intensity and magnetic field region dimensions are intended to be determined. The verifications of the results are verified with a real system. Two scenarios are proposed and for each one two distinct analyses are held. Electromagnet and magnetic flux analyses are held with finite element simulator.**

Keywords—helmholtz; hall-effect; homogenity; measurement; magnetic flux

I. INTRODUCTION

As the robot size decreases, it gets difficult to add functions (battery, wireless charging function, adding a controller or actuator for movement). Thus, acting a force by using an external effect is one of the solutions for this challenge. Also, the reduction of the robot size causes the force effecting to the robot to decrease and makes it difficult to control with the ratio of the disturbances. This kind of microrobot control theory primarily depends on the current flowing through the electromagnet coils. For the motion control, the gradient of the magnetic field plays an active role generating the force.

Actuator positions, numbers and movement mechanisms affect the degrees of freedom [4]. Moreover, the actuator size and positioning do not let it operate on all the parts of the human body. Another disadvantage is the working area of the robot is narrow due to the actuator structures and positioning. Micro robot physical architecture affected by the liquid of operation field also affects the movement performance of the robot.

Electromagnets are coil structures showing magnet features when current is applied. The magnetic flux lines and magnetic flux density show changes depending on the current, the diameter and the winding of copper wire. A ferromagnetic core is positioned inside the coil to concentrate the flux lines to generate more intense magnetic field.

Electromagnets are used in many applications in daily life as actuators, though in medical and academic applications, especially MRI devices, contactless power transmission and contactless robot control presented by Floyd and his colleagues did on a flat surface [5]. Helmholtz electromagnet couple is used for generating homogenous magnetic field in the workspace between the coils, where the robot control is realized. A Helmholtz electromagnet couple example is given in Figure 1.

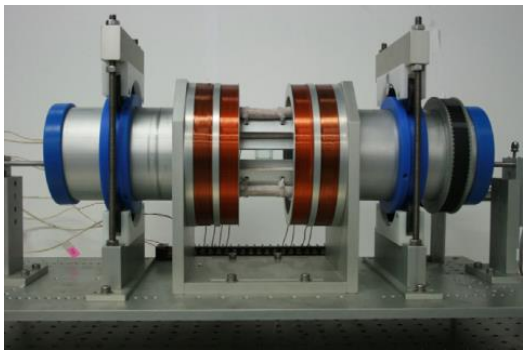

Fig. 1. A Helmholtz electromagnet couple [6].

A. Problem Definition

The dimensions of the identical workspace may vary depending on the structural design of the electromagnet, which would be very critical for the first step of a project. Even the electromagnet positions might be adjustable, the cores and the coils being unmodifiable, affect the working space dimensions. Also, the electromagnet positions may have constraints depending on the construction.

Depending on the requirement for the system, the required or optimal magnetic field values or coil distances may vary. Thus, the electromagnet optimization can be carried out individually for each requirement.

This work is financially supported by the Scientific and Technology Research Council of Turkey (TÜBITAK, Grant no. 215M879).

In this study, the electromagnet optimization is based on *2-D* plane. The relationship of electromagnet design outputs with different sizes and distances are handled.

In the literature, generally basic models like air or cylindrical iron cores are formulized. Complex core structures make it difficult to use the conventional calculation. For these calculations, a finite element simulator is used.

II. Materials And Methods

Depending on the fundamentals of physics, the torque affecting the microrobot is given in (1).

$$\tau = v(M \times B) \tag{1}$$

Where *M* refers magnetization, *v* refers volume and *B* refers magnetic field strength. *v* and *M* are constant because of the microrobot's geometrical and material characteristics. The magnetic field is the only variable which is controllable in the control system as seen in (1).

The electromagnet design which is given in Figure 2 is decided to be with cuboid core and cylindrical coil for having a cubic shaped workspace. This study deals with this structure model and handles width, height and coil radius variables for the study.

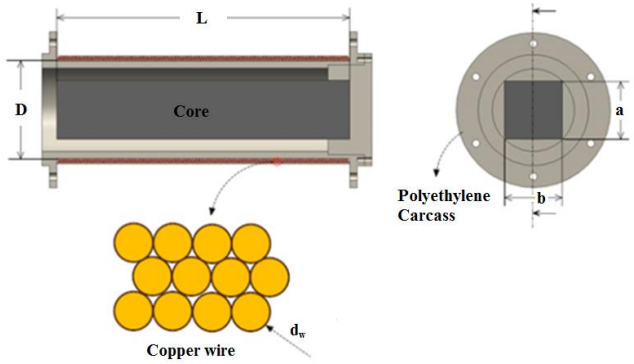

Fig. 2. Electromagnet structure.

Here, *D* refers to copper wire diameter, *L* refers to the length of the electromagnet, d_w refers to the diameter of the wire, *a* and *b* refer the cross-section dimensions of the core.

The generated magnetic field with a coil can be formulized using Biot-Savart law, which is given in (2). Depending on this fundamental law, the magnetic field caused by the current flowing cable can be calculated.

$$d\vec{B} = \frac{\mu_0}{4\pi} \frac{Id\vec{L} \times \vec{l}_r}{4\pi r^2} \tag{2}$$

Where μ_0 refers to permeability of space, *I* refers to current, *L* refers to the length of conductor, $\vec{l}_r$ refers to the vector pointing to the field point and *r* refers to the distance to the field point.

A. Finite Element Simulation

The simulations are held in COMSOL Multiphysics finite element simulation program. This program has multi-physics integration feature that enables to simulate the system using augmented physics-based modules. Thus, it can generate the desired variables as output depending on the canons picked before the simulation computation. It is believed to use finite element method simulators with complex structures for approximate and fast results.

For the simulations in COMSOL, Ampere's Law physics canon is used with steady state study. The equations defined in this law are given in (3), (4) and (5).

$$\nabla \times H = J \tag{3}$$

$$B = \nabla \times A \tag{4}$$

$$J = \sigma.E \tag{5}$$

Where *H* refers to magnetic field vector and *J* refers to external current density, which is used to express the relationship between the magnetic field and electric field. The others variables *A* refers to magnetic field potential, σ refers to charge density and *E* refers to electric field.

The base model designed in COMSOL is given in Figure 3. The assumption is that currents flowing through the copper wires have the same value for both electromagnet coils, where they have their individual power supplies in practice. In the middle of the box, the workspace can be observed. This should not be forgotten that the analyses results are collected and evaluated just for a plane.

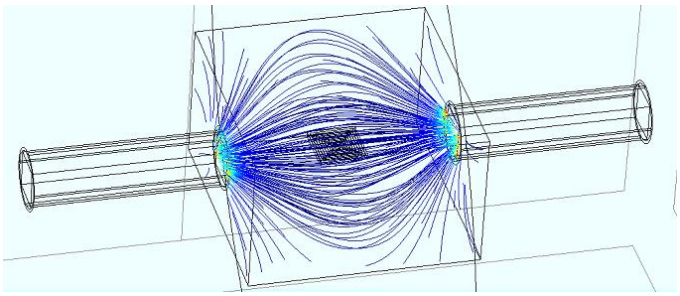

Fig. 3. Helmholtz simulation couple with magnetic fluxlines.

In any simulation, the meshing process plays the key role for precise results. As the size of mesh element is smaller, the results get more accurate, with the disadvantage of the computing load.

The middle box is picked as the measurement space where the meshes are tighter for simulating the best magnetic flux lines. For the measurement readings, some rectangular contours are added.

B. *Magnetic Field Measurement*

Hall effect sensors are transducers that convert magnetic field into voltage. When a magnetic field perpendicular to hall material face is applied, as some current flows through the direction perpendicular to the material face, a voltage is generated between the remaining two faces.

Hall effect based measurement is a common way for detecting the amplitude of the magnetic flux. Due to having small dimensions, wide bandwidth, large range and high linearity, hall effect sensor based measurements are reliable. As the measurement workspace is not so large, the dimensions are ideal for hall effect sensor usage.

The measurements are held to clarify the simulation results with the realized system. The measurements are held by a professional and precise gauss meter, F.W. Bell 5180, manufactured by F. W. Bell.

For the verification, a case study is held. A couple of Helmholtz electromagnets is used in this process which is shown in Figure 4. The case in the middle of the system is the workspace where the magnetic field is generated for robot control. There should not be any confusion about that only two electromagnets are used facing to each other, the other electromagnets are inactive. The cores have dimensions of 40mm x 40mm with a depth of 200 mm. There are 600 turns of copper wire, with 3 layers where 200 turns for each one. The inner radius is 33 mm, considering a constant plastic carcass space between the core and the copper. The distance is set to 180 mm between two coils and the current values are set to 4 A.

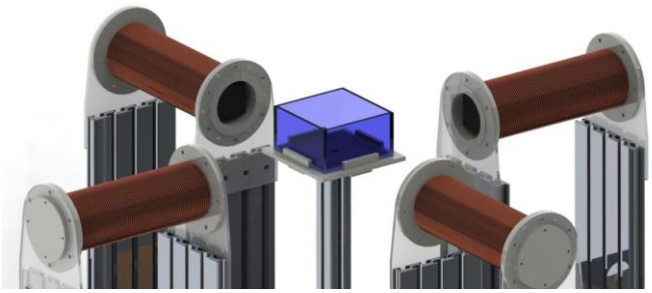

Fig. 4. The measurement set.

III. Initial Measurements

Using COMSOL, the simulation outputs are given in Figure 5. At the top and the bottom sides of the figure, active electromagnets can be observed. The origin of the working space at (0,0) is simulated with the output 5,589 *mT*. All the region boundaries are determined depending on this midpoint magnetic field strength value. Purple region represents the magnetic field having a magnetic field with the value between 105% and 95% of (0,0) point, named 1st region. As following, green region represents the interval between 95% and 90%, named 2nd region and brown region represents the interval between 90% and 80%, named 3rd region.

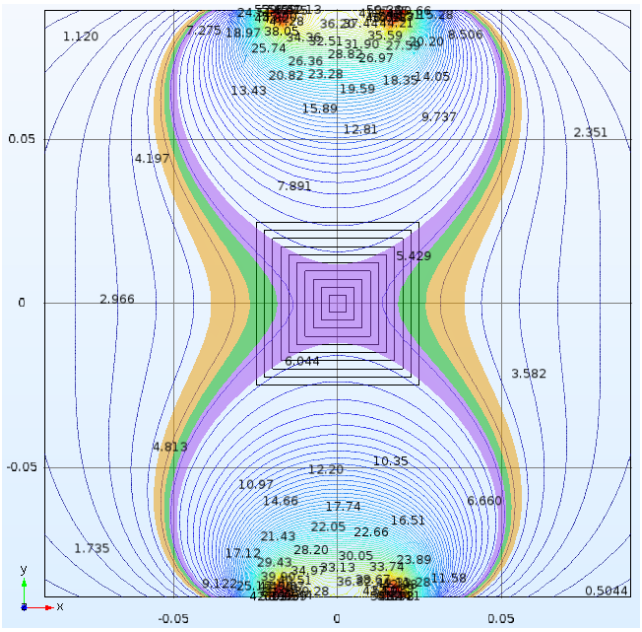

Fig. 5. Magnetic field verification case output in the middle layer with the top view generated by COMSOL.

As the results are compared using gauss meter measurements, the simulation outputs are observed to be identical. The magnetic field areas are having distinction at the expected boundary distances with boundary values.

Also, as estimated, the magnetic field's magnitude changes proportionally with the current value. Change in the magnitude of the current does not change the boundaries of regions. So, the considered regions only depend on the electromagnet structure, not to the current's amplitude. The same magnetic field value can be obtained by changing the current with different core dimensions. Thus, when the electromagnets are integrated into a control system, the desired magnetic field can be generated with different core structures, but with different current values, where we can also talk about the efficiency of the electromagnets.

IV. Simulation Results

Two different simulation scenarios are held with two different constraints.

First scenario constraint is that, the electromagnets are planned to be placed on a mobile platform and the weight of the electromagnets are limited. A basic assumption is made as the weight is mainly derived of the core weight because of its large volume. One of the other weight reasons, the copper weight, is ignored because the magnetic field strength can be compensated by just changing the current value. For an easier comparison, the core weights are counted as 2,520 kg as the same core weight of the manufactured system where the verification measurements are accomplished. A parametric simulation is held and the results are given in Table 1 where distance refers the distance between two coils, C_w refers the width of the core, C_h refers the height of the core, R_{inner} refers

the inner core radius and *mf* refers the magnetic field strength at the point (0,0) along *y* axes. The evaluated distances with the colored areas are the distances along *x* axes between their outer sides and the point (0,0).

TABLE I. SCENARIO-1 SIMULATION RESULTS.

Distance = 16 mm						
C_w (mm)	C_h (mm)	R_{inner} (mm)	mf (mT)	1st region (mm)	2nd region (mm)	3rd region (mm)
10	160	160,3	9,22	19,5	28	41
20	80	82,5	7,72	17,5	24,5	35,5
30	53,3	61,2	7,16	17,5	24,5	35,5
40	40	56,6	7,03	17,5	25	36
50	32	59,4	7,11	17,5	25	37
60	26,7	65,7	7,28	18,5	26,5	39
70	22,9	73,6	7,49	18,5	27	39,5
80	20	82,5	7,72	20	28,5	40,5
90	17,8	91,7	7,95	21	29,5	43,5
100	16	101,3	8,18	21,5	32	45,5
Distance = 18 mm						
C_w (mm)	C_h (mm)	R_{inner} (mm)	mf (mT)	1st region (mm)	2nd region (mm)	3rd region (mm)
10	160	160,3	7,81	21,5	29,5	44
20	80	82,5	6,35	19	26	39
30	53,3	61,2	5,83	18,5	26,5	38,5
40	40	56,6	5,71	19	27	38,5
50	32	59,4	5,79	18,2	26,2	40
60	26,7	65,7	5,94	18,5	28,5	41
70	22,9	73,6	6,14	19,7	30	41,5
80	20	82,5	6,35	22	30	43,5
90	17,8	91,7	6,57	23,5	32	45,5
100	16	101,3	6,79	24,1	33,5	47
Distance = 20 mm						
C_w (mm)	C_h (mm)	R_{inner} (mm)	mf (mT)	1st region (mm)	2nd region (mm)	3rd region (mm)
10	160	160,3	6,49	22,5	31,5	46
20	80	82,5	5,07	20	28,5	41,5
30	53,3	61,2	4,62	19	27	41,5
40	40	56,6	4,52	20	29	42
50	32	59,4	4,58	20	30	43
60	26,7	65,7	4,71	22,5	28,5	43,5
70	22,9	73,6	4,88	22,5	30	43,5
80	20	82,5	5,07	22	30,5	46
90	17,8	91,7	5,26	24,5	34	48
100	16	101,3	5,46	9	27,5	43
Distance = 22 mm						
C_w (mm)	C_h (mm)	R_{inner} (mm)	mf (mT)	1st region (mm)	2nd region (mm)	3rd region (mm)
10	160	160,3	5,61	23,5	34,5	49,5
20	80	82,5	4,29	21,5	30	45
30	53,3	61,2	3,88	20,5	30,5	43,5
40	40	56,6	3,80	23	31	45
50	32	59,4	3,85	22,5	32	46,5
60	26,7	65,7	3,97	20	32,5	47,5
70	22,9	73,6	4,12	24,5	32,5	48
80	20	82,5	4,29	23	32,5	48
90	17,8	91,7	4,47	22,5	33,5	49,5
100	16	101,3	4,65	25	36	52,5

The second scenario constraint for the analysis is that the inner radius for the copper wire is held constant as 56,6 mm equal to the inner coil radius of the manufactured system. So, the height of the core varies with the width value of the core. The simulation results are given in Table 2. Also, as expected, the core width range is not as wide as in the first scenario.

TABLE II. SCENARIO-2 SIMULATION RESULTS.

Distance = 16 mm					
C_w (mm)	C_h (mm)	mf (mT)	1st region (mm)	2nd region (mm)	3rd region (mm)
20	52,9	6,38	16,5	23,5	34,5
30	48	6,85	16	24	35
40	40	7,03	17,5	25	35,5
50	26,5	6,71	17,5	25	37,5
Distance = 18 mm					
C_w (mm)	C_h (mm)	mf (mT)	1st region (mm)	2nd region (mm)	3rd region (mm)
20	52,9	5,08	17,5	25	37,5
30	48	5,45	18,5	26,5	37,5
40	40	5,59	18,5	27	38,5
50	26,5	5,34	20	28	39
Distance = 20 mm					
C_w (mm)	C_h (mm)	mf (mT)	1st region (mm)	2nd region (mm)	3rd region (mm)
20	52,9	4,11	20	27	40
30	48	4,41	18,5	27	41
40	40	4,52	20	28	41,5
50	26,5	4,32	21,5	29	42,5
Distance = 22 mm					
C_w (mm)	C_h (mm)	mf (mT)	1st region (mm)	2nd region (mm)	3rd region (mm)
20	52,9	3,38	22,5	28,5	43
30	48	3,62	22	28,5	44,5
40	40	3,71	20,5	31,5	44
50	26,5	3,54	20,5	30,5	45

V. DISCUSSION

An optimization process is required for determining the most optimal dimensions for the system. For a conventional optimization method, using a transfer function, the maxima point may give the optimal point. For this problem, in the first scenario, two inputs (distance and core width) and five outputs (coil inner radius, magnetic field in *y* direction, first/second/third region boundary distances), in the second case, two inputs and four outputs exist (coil inner radius is constant). For this reason, an optimization formula should be evaluated. A basic optimization formulation, *J*, is proposed as in (6) where w_a refers weight of advantages, w_d refers the weight of disadvantages and *k* refers the number of cases.

$$J = \sum_{n=1}^{k} \frac{\prod w_{a,n}}{\prod w_{d,n}} \tag{6}$$

Here, the weights of the variables may depend on the user in accordance with the priorities, so that there are many true solutions for this function.

For both scenarios, one approach is to give same weight to the outputs. All the region distances and magnetic field values influence to the function positively and the coil radius effects negatively. For the second scenario, as the coil radius is constant, all the remaining outputs influence as positive effects. Also, summing operation can be used for each distance results.

For the first scenario, a formula is proposed in (7). As three regions are handled, for the second and the third regions, their

ratios with the first region size is taken into consideration to prevent inequality, or the first region size affects the region by power of three. The results are given in Table 3. Here, the distances are assumed to be used in summing operation.

$$J = \sum_{n=16,n+=2}^{22} \frac{\prod mf_n.d_{1,n}.\frac{d_{2,n}}{d_{1,n}}.\frac{d_{3,n}}{d_{1,n}}}{R_{inner,n}} \quad (7)$$

TABLE III. FIRST SCENARIO - FIRST PROPOSAL RESULTS.

C_w (mm)	Distance				J_{Total}
	16 mm	18 mm	20 mm	22 mm	
10	3,38474	2,9429	2,6062	2,5423	11,47637
20	4,65279	4,1108	3,6346	3,2668	15,66508
30	5,81234	5,2543	4,4531	4,1075	19,62736
40	6,38841	5,5258	4,8688	4,0701	20,85328
50	6,32995	5,6141	4,9811	4,2905	21,21583
60	6,19142	5,7139	3,9559	4,6642	20,52557
70	5,86599	5,2696	3,8469	3,5646	18,54716
80	5,40297	4,5687	3,9195	3,5285	17,41981
90	5,29740	4,4368	3,8212	3,5891	17,14468
100	5,47093	4,3787	7,0841	3,4705	20,40441

As seen, for C_w = 50 mm, the best result is acquired. Also, the results are obtained with closer values that are not desired for a clear determination. For a second analysis, the coil radius effect is increased as the power of two to the proposed formula because as the radius increases, the copper winding weight increases proportionally which is not desired for the scenario constraint. Moreover, the ergonomics of the system effect negatively as larger coil is used, larger volume it will consume. When thought about a system with four coils as shown in Figure 4, the coil dimension obstructs closer distances between the electromagnets. In (8), the second optimization analysis formulation is given and results are shown in Table 4.

$$J = \sum_{n=16,n+=2}^{22} \frac{\prod mf_n.d_{1,n}.\frac{d_{2,n}}{d_{1,n}}.\frac{d_{3,n}}{d_{1,n}}}{R_{inner,n}^2} \quad (8)$$

TABLE IV. FIRST SCENARIO - SECOND PROPOSAL RESULTS.

C_w (mm)	Distance				J_{Total}
	16 mm	18 mm	20 mm	22 mm	
10	0,02111	0,0183	0,0162	0,0158	0,071587
20	0,05642	0,0498	0,0440	0,0396	0,189967
30	0,09498	0,0858	0,0727	0,0671	0,320751
40	0,11293	0,0976	0,0860	0,0719	0,368637
50	0,10663	0,0945	0,0839	0,0722	0,357389
60	0,09429	0,0870	0,0602	0,0710	0,312608
70	0,07966	0,0715	0,0522	0,0484	0,251871
80	0,06552	0,0554	0,0475	0,0427	0,211246
90	0,05774	0,0483	0,0416	0,0391	0,186885
100	0,05402	0,0432	0,0699	0,0342	0,201481

Here, the differences between the results are more distinctive than the first proposal with the change of the weights. For 40 and 50 mm core width inputs, the results have the largest values and for 40 mm, the function has the top value. To conclude, the first scenario constraints the core weight and with the second formula proposal, the negative effect of the radius is increased and more clear results are obtained.

For the second scenario, where the constraint is the winding radius, a similar formulation is proposed in (9). The results are given in Table 5.

$$J = \sum_{n=16,n+=2}^{22} \prod mf_n.d_{1,n}.\frac{d_{2,n}}{d_{1,n}}.\frac{d_{3,n}}{d_{1,n}} \quad (9)$$

TABLE V. SECOND SCENARIO - FIRST PROPOSAL RESULTS.

C_w (mm)	Distance				J_{Total}
	16 mm	18 mm	20 mm	22 mm	
20	313,598	272,01	221,91	183,94	991,4809
30	359,362	292,49	263,65	208,43	1123,946
40	356,338	314,04	262,76	250,92	1184,069
50	359,421	291,42	247,58	237,30	1135,740

Here, the differences between the results are still not far enough for a clear determination. As the radius is constant, region distance effects are boosted as in (10) with a direct effect instead of a ratio metric relationship and the results are given in Table 6.

$$J = \sum_{n=16,n+=2}^{22} \prod mf_n.d_{1,n}.d_{2,n}.d_{3,n} \quad (10)$$

TABLE VI. SECOND SCENARIO - SECOND PROPOSAL RESULTS.

C_w (mm)	Distance				J_{Total}
	16 mm	18 mm	20 mm	22 mm	
20	85377,0	83306,0	88767,3	93122,0	350572,5
30	91996,8	100106,5	90234,7	100883,4	383221,5
40	109128,7	107480,6	105107,5	105449,1	427166,1
50	110072,8	116571	114448,1	99726,1	440818,0

Here, the differences between the results are more distinct than the first proposal with the change of the weights. For 40 and 50 mm core width inputs, the results have the largest values and for 50 mm, the function has the top value. To conclude, the second scenario constraints the coil radius and with the second formula proposal, the positive effect of the region distances are increased and more clear results are obtained.

VI. Conclusion

In this paper, the optimization of Helmholtz electromagnet design is considered. The core and coil designs are picked with a cuboid and cylindrical geometry respectively and all the works are built on this structure dimensions. The simulation results and real values are compared and verified. Two scenarios with different constraints are given and for each one, two optimization formulas are proposed.

The results show that the optimization formulation with varying weights depending on the desired priorities for the system make the formulation more accurate and optimal. Here, with the first scenario, the radius of the coil is preferred that will apply larger negative effect and changes the weight by the power of two with the secondly proposed formulation. In the second scenario, the homogeneity regions are decided to make greater effect and increased the weight on the secondly proposed formulation. As seen, for C_w = 40 mm and C_w = 50 mm can be picked optimal for the system with the formulations proposed.

This work has only *y*-axes component of the magnetic field generated at the workspace as input to the formulation. It should also be considered that the magnetic field may include the other components as the purity of the desired fields. Furthermore, the distances on *x*-axes are considered as the outputs on *x*-*y* plane. Using additional output values in spatial points may improve the formulation. These issues will be considered in future studies.

VII. Acknowledgement

This work is financially supported by the Scientific and Technology Research Council of Turkey (TÜBITAK, Grant no. 215M879). We would also like to thank Smart Structures Laboratory of Ege University Department of Mechanical Engineering for providing the support of using COMSOL program and for the very useful reviews of the anonymous reviewers.

References

[1] S. Jeong, H. Choi, S. Y. Ko, J. O. Park, and S. Park, “Remote controlled micro-robots using electromagnetic actuation (EMA) systems”, 2012 4th IEEE RAS & EMBS International Conference on Biomedical Robotics and Biomechatronics (BioRob), pp. 482-487, 2012.

[2] J. B. Mathieu, S. Martel, L. H. Yahia, G. Soulez, and G. Beaudoin, “Preliminary investigation of the feasibility of magnetic propulsion for future
microdevices in blood vessels”, Bio-Medical Materials and Engineering, vol. 15(5), pp.367-374, 2005.

[3] Y. Haga, and M. Esashi, “Biomedical microsystems for minimally invasive diagnosis and treatment”, Proceedings of the IEEE, vol. 92(1), pp. 98-114, 2004.

[4] M. P. Kummer, J.J. Abbott, B. E. Kratochvil, R. Borer, A. Sengul, and B. J. Nelson, “OctoMag: An electromagnetic system for 5-DOF wireless micromanipulation”, IEEE Transactions on Robotics, vol. 26(6), pp. 1006-1017, 2010.

[5] S. Floyd, C. Pawashe, and M. Sitti, "An untethered magnetically actuated micro-robot capable of motion on arbitrary surfaces", Robotics and Automation, ICRA 2008, IEEE International Conference on IEEE, pp. 419-424, 2008.

[6] H. Choi, K. Cha, J. Choi, S. Jeong, S. Jeon, G. Jang, S., J. Park, and S. Park, “EMA system with gradient and uniform saddle coils for 3D locomotion of microrobot”, Sensors and Actuators A: Physical, vol. 163(1), pp. 410-417, 2010.